Available online at www.sciencedirect.com
SCIENCE DIRECT®
International Journal of Heat and Mass Transfer 47 (2004) 1257–1266
International Journal of HEAT and MASS TRANSFER
www.elsevier.com/locate/ijhmt

Non-Darcy flow stability of mixed convection in a vertical channel filled with a porous medium

Yen-Cho Chen *

Department of Mechanical Engineering, Oriental Institute of Technology, No. 58, Sze-Chuan Road, Sec 2, Panchiao 220, Taiwan, ROC

Received 11 June 2003; received in revised form 6 September 2003

Abstract

The linear stability analysis of mixed convection in a heated vertical channel filled with a porous medium was investigated. The Galerkin method was employed in this calculation. The results indicated that the fully developed laminar flow could become unstable under a mild heating condition for higher modified Darcy numbers of $Da^* = 1$ and 10^{-2}, but the critical Rayleigh number increases substantially for $Da^* = 10^{-4}$. The disturbance kinetic energy budget analysis showed that, for $Da^* = 1$ and 10^{-2}, there are generally three instability types, the thermal-buoyant, mixed, and thermal-shear instabilities for low, intermediate, and high Reynolds numbers, respectively, while for $Da^* = 10^{-4}$, the thermal-buoyant instability is the only driving mechanisms of flow instability regardless of the value of Reynolds number.

Keywords: Non-Darcy flow; Linear stability; Mixed convection

1. Introduction

The fluid flow and heat transfer in the wall-bounded forced flow through a porous medium has been extensively studied in the past, because it relates to various applications such as solid matrix heat exchanger, thermal insulation, nuclear waste disposal, geothermal energy extraction, thermal energy storage in underground aquifers, and other practical interesting designs. In the laminar forced convection in a porous channel, Vafai and Kim [1] presented an exact solution for the velocity and temperature fields by using Darcy–Brinkman–Forchheimer (DBF) model. They showed that for a high-permeability porous medium the thickness of the momentum boundary layer depends on both the Darcy number and the inertia parameter, and neglecting the inertia effect could lead to serious errors for Nusselt number calculations. Nield et al. [2] also presented a theoretical analysis of fully developed forced convection in a porous channel. They indicated that their general solution, with no restrictions, extends existing solutions to all values of the Darcy number and Forchheimer inertia coefficient, and also to a medium with the effective viscosity different from the fluid viscosity. Hadim and Chen [3] investigated the non-Darcy mixed convection in a vertical porous channel with asymmetric wall heating. Their results showed that as the Darcy number is decreased, distortions in the velocity profile lead to increased heat transfer. The fully developed mixed convection in a vertical porous channel with imposed uniform heat flux was performed using DBF model by Chen et al. [4]. It was shown that the buoyancy force can significantly affect Nusselt number for higher Rayleigh numbers, higher modified Darcy number and/or lower Forchheimer number. A comprehensive review in the laminar wall-bounded forced or mixed convection is given by Nield and Bejan [5].

The linear stability of natural convection in a permeable medium between vertical coaxial cylinders was investigated by Bau and Torrance [6]. They found that

* Tel.: +886-29610145x331; fax: +886-277386648.
E-mail address: ycchen@mail.oit.edu.tw (Y.-C. Chen).

0017-9310/$ - see front matter © 2003 Elsevier Ltd. All rights reserved.
doi:10.1016/j.ijheatmasstransfer.2003.09.010

Nomenclature

c	complex wave speed ($= c_r + \mathrm{i}c_i$)
c_F	inertial coefficient
C_1	axial temperature gradient
Da^*	modified Darcy number, $\mu_e K/\mu_f L^2$
E_s, E_b, E_d	disturbance kinetic energies
E_F, E_{Da}	defined in Eq. (15)
$\vec{e}_x$	unit vector in the x direction
F	Forchheimer number, $c_F LG/\sqrt{K}$
g	gravitational acceleration
G	pressure gradient, $-\mathrm{d}p_B/\mathrm{d}x$
K	permeability
L	half width of channel
p	pressure
Pr	effective Prandtl number, ν_e/α_e
Ra	Rayleigh number, $g\beta_T C_1 L^4/\nu_e\alpha_e$
Re	Reynolds number
S	ratio of effective to fluid thermal Capacitance, $(\rho c)_e/(\rho c)_f$
t	time
T^*	dimensional temperature
T_w^*	dimensional wall temperature
U_B	velocity at laminar base state
$\vec{V}$	fluid velocity
u, v, w	flow velocity components
x, y, z	coordinates

Greek symbols

α	streamwise wave number
α_e	effective thermal diffusivity
β	spanwise wave number
β_T	thermal expansion coefficient
ε	porosity
θ	dimensionless temperature
θ_B	temperature at laminar base state
μ_e	effective viscosity
μ_f	fluid viscosity
ν_e	effective kinematic viscosity
ρ_f	fluid density

Superscripts

*	dimensional quantity
$'$	infinitesimal disturbance
$\wedge$	complex amplitude function of disturbance, defined in Eq. (8)

Subscript

B	at laminar base state

the preferred convective modes at the onset of convection are predominantly asymmetric. Kladias and Prasad [7] studied the flow transition of the natural convection in a porous medium heated from below by DBF model. They found that at the onset, the oscillatory convection is highly periodic, but with an increase in convective motions the disorder increases monotonically and the fluctuations become highly random. The linear stability and flow transition of mixed convection in simple geometries such as pipe and channel with or without porous medium are fundamental issues in heat transfer and fluid dynamics. This research topics in the channel flows for the pure viscous fluid were examined by Chen and Chung [8,9]. For a flow configuration in a vertical heated porous channel, it is desired to know whether the flow is stable or not, and the flow instability driving mechanism. Thus the linear stability analysis was investigated in this paper.

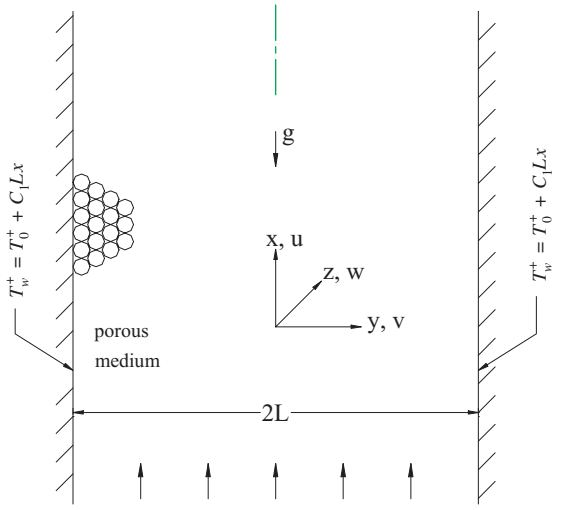

Fig. 1. The schematic of geometry and coordinate system.

2. Formulation

The problem under investigation is the fully developed mixed convection between two parallel vertical plates filled with a fluid-saturated porous medium. The uniform heat flux is symmetrically imposed on both walls. The schematic of this system is given in Fig. 1. The mathematical model of the non-Darcy flow proposed by Kladias and Prasad [7] was generally followed. The governing equations for continuity, momentum, and energy could be written as:

$$\nabla^* \cdot \vec{V}^* = 0 \tag{1}$$

$$\frac{\rho_f}{\varepsilon}\frac{\partial \vec{V}^*}{\partial t^*}+\frac{\rho_f}{\varepsilon^2}(\vec{V}^*\cdot\nabla^*)\vec{V}^* = -\nabla^* p^* - \frac{\mu_f}{K}\vec{V}^* - \rho_f \frac{c_F}{\sqrt{K}}|\vec{V}^*|\vec{V}^* + \rho_f g\vec{e}_x + \mu_e \nabla^{*2}\vec{V}^* \tag{2}$$

$$S\frac{\partial T^*}{\partial t^*} + (\vec{V}^*\cdot\nabla^*)T^* = \alpha_e \nabla^{*2} T^* \tag{3}$$

It is noted that Kladias and Prasad wrote the Forchheimer term as $b|\vec{V}^*|\vec{V}^*/K$, where b is the porous matrix structure property associated with inertia term. For a constant heat flux at the walls, the wall temperature is assumed to increases linearly with x^* as $T_w^* = T_0^* + C_1 x^*$, where C_1 is the axial temperature gradient, and T_0^* is the upstream reference wall temperature. Here μ_e in Eq. (2) is called as the apparent viscosity [7] or effective viscosity [10] for Brinkman's term. Discussions on the value of μ_e could be found in the Refs. [10,11]. The non-dimensionalization is carried out based on the following definition.

$$x = \frac{x^*}{L}, \quad y = \frac{y^*}{L}, \quad z = \frac{z^*}{L}, \quad p = p^*\frac{L^2}{\rho_f v_e^2} \tag{4a}$$

$$t = t^*\frac{v_e G}{L^2}, \quad \vec{V} = \frac{\vec{V}^* L}{v_e}\frac{1}{G}, \quad \theta = \frac{T^* - T_w^*}{C_1 L G Pr} \tag{4b}$$

where $G = -\mathrm{d}p_B/\mathrm{d}x$ is the pressure gradient at laminar state. The dimensionless momentum and energy equations are

$$\frac{G}{\varepsilon}\frac{\partial \vec{V}}{\partial t} + \frac{G}{\varepsilon^2}(\vec{V}\cdot\nabla)\vec{V} = -\frac{1}{G}\nabla p - \frac{1}{Da^*}\vec{V} - F|\vec{V}|\vec{V} + Ra\,\theta\vec{e}_x + \nabla^2\vec{V} \tag{5}$$

$$S\frac{\partial\theta}{\partial t} + u\frac{\partial\theta}{\partial x} + v\frac{\partial\theta}{\partial y} + w\frac{\partial\theta}{\partial z} = \frac{1}{GPr}(\nabla^2\theta - u) \tag{6}$$

The Boussinesq approximation is used in Eq. (5). Here $Da^* = \mu_e K/\mu_f L^2$ is the modified Darcy number, $F = c_F L G/\sqrt{K}$ is the Forchheimer number, and $Ra = g\beta_T C_1 L^4/v_e\alpha_e$ is the Rayleigh number.

In the linear stability analysis, the infinitesimal disturbances are imposed on the fully developed laminar base flow, thus the velocity, pressure, and temperature fields can be written as:

$$\vec{V} = U_B(y)\vec{e}_x + \vec{V}', \quad p = p_B(x) + p', \quad \theta = \theta_B(y) + \theta' \tag{7}$$

where U_B, p_B, and θ_B refers to the flow velocity, pressure, and temperature at laminar base state, respectively. The laminar velocity and temperature profiles can be found in Fig. 3 of Ref. [4]. There are errata in captions in Ref. [4], where the caption of Fig. 1 should be entirely exchanged with that of Fig. 2. The prime in Eq. (7) denotes the infinitesimal disturbances. By using the usual normal mode form, the disturbances can be represented by

$$\begin{aligned}\vec{V}' &= \hat{\vec{V}}(y)e^{i(\alpha x+\beta z-\alpha ct)}\\ p' &= \hat{p}(y)e^{i(\alpha x+\beta z-\alpha ct)}\\ \theta' &= \hat{\theta}(y)e^{i(\alpha x+\beta z-\alpha ct)}\end{aligned} \tag{8}$$

where $\hat{\vec{V}} = (\hat{u},\hat{v},\hat{w})$, $\hat{p}$, and $\hat{\theta}$ are the complex amplitude functions. Here α (real) and β (real) are the wave numbers in the x and z directions, respectively, and $c = c_r + ic_i$ is the complex wave speed. The growth or decay of the disturbance depends on c_i. The flow is stable, neutrally stable, or unstable for $c_i < 0$, $c_i = 0$, or $c_i > 0$, respectively. Following the standard linear stability method [8], the linearized stability equations become the following:

$$\begin{aligned}&\frac{\mathrm{d}^4\hat{v}}{\mathrm{d}y^4} - 2(\alpha^2+\beta^2)\frac{\mathrm{d}^2\hat{v}}{\mathrm{d}y^2} + (\alpha^2+\beta^2)^2\hat{v}\\ &\quad + i\alpha\frac{G}{\varepsilon^2}\left[-U_B\frac{\mathrm{d}^2\hat{v}}{\mathrm{d}y^2} + \frac{\mathrm{d}^2U_B}{\mathrm{d}y^2}\hat{v} + (\alpha^2+\beta^2)U_B\hat{v}\right]\\ &\quad + \frac{1}{Da^*}\left[-\frac{\mathrm{d}^2\hat{v}}{\mathrm{d}y^2} + (\alpha^2+\beta^2)\hat{v}\right] - \left(\frac{\alpha^2}{\alpha^2+\beta^2}+1\right)\\ &\quad \times F\frac{\mathrm{d}}{\mathrm{d}y}\left(|U_B|\frac{\mathrm{d}\hat{v}}{\mathrm{d}y}\right) + (\alpha^2+\beta^2)F|U_B|\hat{v}\\ &\quad + \frac{i\alpha\beta}{\alpha^2+\beta^2}F\frac{\mathrm{d}}{\mathrm{d}y}(|U_B|\hat{\eta}) - i\alpha Ra\frac{\mathrm{d}\hat{\theta}}{\mathrm{d}y}\\ &\quad = i\alpha c\frac{G}{\varepsilon}\left[-\frac{\mathrm{d}^2\hat{v}}{\mathrm{d}y^2} + (\alpha^2+\beta^2)\hat{v}\right]\end{aligned} \tag{9}$$

$$\begin{aligned}&-\frac{\mathrm{d}^2\hat{\eta}}{\mathrm{d}y^2} + (\alpha^2+\beta^2)\hat{\eta} + i\alpha\frac{G}{\varepsilon^2}U_B\hat{\eta} + \beta\frac{G}{\varepsilon^2}\frac{\mathrm{d}U_B}{\mathrm{d}y}\hat{v}\\ &\quad + \frac{1}{Da^*}\hat{\eta} + \left(\frac{\beta^2}{\alpha^2+\beta^2}+1\right)F|U_B|\hat{\eta}\\ &\quad + \frac{i\alpha\beta}{\alpha^2+\beta^2}F|U_B|\frac{\mathrm{d}\hat{v}}{\mathrm{d}y} - \beta Ra\hat{\theta}\\ &\quad = i\alpha c\frac{G}{\varepsilon}\hat{\eta}\end{aligned} \tag{10}$$

$$\begin{aligned}&\frac{1}{GPr}\left[-\frac{\mathrm{d}^2\hat{\theta}}{\mathrm{d}y^2} + (\alpha^2+\beta^2)\hat{\theta}\right] + i\alpha U_B\hat{\theta}\\ &\quad + \frac{\mathrm{d}\theta_B}{\mathrm{d}y}\hat{v} + \frac{1}{GPr(\alpha^2+\beta^2)}\left(i\alpha\frac{\mathrm{d}\hat{v}}{\mathrm{d}y} + \beta\hat{\eta}\right)\\ &\quad = i\alpha cS\hat{\theta}\end{aligned} \tag{11}$$

where $\hat{\eta} = \beta\hat{u} - \alpha\hat{w}$. The associated boundary conditions are

$$\hat{v} = \frac{\mathrm{d}\hat{v}}{\mathrm{d}y} = \hat{\eta} = \hat{\theta} = 0 \quad \text{at } y = \pm 1 \tag{12}$$

Eqs. (9)–(11) and the corresponding boundary conditions constitute an eigenvalue problem.

3. Numerical method

The Galerkin method is used to solve the coupled Eqs. (9)–(11) and their associated boundary conditions. In this method, the test (weighted) functions are the same as the base (trial) functions. Thus the $\hat{v}$, $\hat{\eta}$, and $\hat{\theta}$ are expanded in the following:

$$\hat{v} = \sum_{n=0}^{N} a_n \xi_n(y), \quad \hat{\eta} = \sum_{n=0}^{N} b_n \zeta_n(y), \quad \hat{\theta} = \sum_{n=0}^{N} d_n \zeta_n(y) \tag{13}$$

where a_n, b_n and d_n are the unknown coefficients. The base functions are shown in the following:

$$\xi_n(y) = (1-y^2)^2 P_n(y), \qquad \zeta_n(y) = (1-y^2) P_n(y) \tag{14}$$

where each base functions $\xi_n(y)$ and $\zeta_n(y)$ satisfies the boundary conditions and $P_n(y)$ is the Legendre polynomial of order n. The other details can be found in Chen and Chung [8]. We verified our code by comparing with the published results of an isothermal channel flow without porous medium for the case of $Ra = 0$ by setting $\varepsilon = 1$, $F = 0$, and $Da^* \to \infty$. Our isothermal results of the critical Reynolds number, $Re_c = 3848.147$ ($Re_c = 5772.22$, if based on the maximum velocity) and the critical wave number, $\alpha_c = 1.0206$ with $N = 51$ in Eq. (13) agree exactly with those given by Orszag [12].

4. Energy budget analysis

In order to understand the role played by the heat transfer during the flow instability, it is therefore necessary to keep track of the kinetic energy budget for the disturbances. The driving mechanisms of flow instability may be determined by the production and dissipation of disturbance kinetic energy [13,8]. The balance of disturbance kinetic energy for the infinitesimal disturbance is

$$\begin{aligned}
&\frac{G}{\varepsilon}\frac{\partial}{\partial t}\left\langle \frac{1}{2}(|u'|^2+|v'|^2+|w'|^2)\right\rangle \\
&\quad = -\frac{G}{\varepsilon^2}\left\langle u'v'\frac{\mathrm{d}U_B}{\mathrm{d}y}\right\rangle + Ra\left\langle u'\theta'\right\rangle - \frac{1}{Da^*}\left\langle (|u'|^2 \right. \\
&\qquad \left. + |v'|^2+|w'|^2)\right\rangle - F\left\langle |U_B|(|u'|^2+|v'|^2+|w'|^2) \right. \\
&\qquad \left. + |U_B|u'u'\right\rangle - \left\langle (\nabla u')^2+(\nabla v')^2+(\nabla w')^2\right\rangle \\
&\quad = E_s + E_b + E_{Da} + E_F + E_d
\end{aligned} \tag{15}$$

where the bracket $\langle\ \rangle$ implies integration over the volume of the disturbance wave. The first term on the right-hand-side of Eq. (15), E_s, represents the shear production of disturbance kinetic energy. The second term, E_b, represents the disturbance kinetic energy production due to the work done by the thermal-buoyant potential of disturbance temperature field. The third term E_{Da} and fourth term E_F, represent the dissipation of energy through the surface drag associated with the modified Darcy term and form drag associated with the Forchheimer term due to the solid matrix, respectively. The last term, E_d, represents the dissipation of energy through viscosity. On the neutral stability curve $c_i = 0$, the disturbances are neither growing nor decaying, thus the left hand side term (differentiation with time) is zero.

5. Results and discussion

The dimensionless parameters in the governing Eqs. (9)–(11) are the modified Darcy number, Da^*, Rayleigh number Ra, Forchheimer number, F, pressure gradient number G, and effective Prandtl number, Pr. Since the Reynolds number, Re, is often used in the stability analysis for forced and mixed convections, therefore the Re is used as one parameter instead of G by the relation of $G = Re/\overline{U}_B$ from Eq. (4b), where $\overline{U}_B$ is the mean laminar flow velocity. The main objective in this study is to investigate the effect of modified Darcy number and the Forchheimer number on the flow stability for the high porosity medium. In this study, Da^* of 1, 10^{-2}, and 10^{-4} and F of 1, 10^2, and 10^4 are chosen for calculation. The modified Prandtl number of 1 and porosity of 0.9 and thermal capacitance ratio, S, of 1 are used. Because the stable and unstable domains are separated by the neutral stability curve of $c_i = 0$, we will basically present the neutral stability curves for various Da^* and F numbers to demonstrate the characteristics of stability for the flow. We have included both integer and non-integer values of spanwise wave number, β, in this computation. The results show that $\beta = 0$ is always the least stable mode, that is, the least stable disturbances are two-dimensional.

The instability boundaries on the (Re, Ra) plane for $Da^* = 1$ and $F = 1$, 10^2, and 10^4 are plotted in Fig. 2. The results show that the critical Rayleigh number, Ra_c, is smaller than 55 for $F = 1$ or 10^2, when Reynolds number is greater than 100. The Ra_c for $F = 10^4$ is smaller than 290 for $Re > 200$. This indicates that the fully developed flow for higher modified Darcy number could become unstable under a very mild heating condition and the buoyancy force has an important effect on the flow instability. The critical Rayleigh number decreases with increasing Re, but the decreasing rate becomes smaller for higher Re. Two curves for $F = 1$ and 10^2 are almost overlapping for $Re > 700$. It is also seen that the variation of the Ra_c between $F = 10^2$ and 10^4 is less than 250 at the same Re, when Reynolds number is

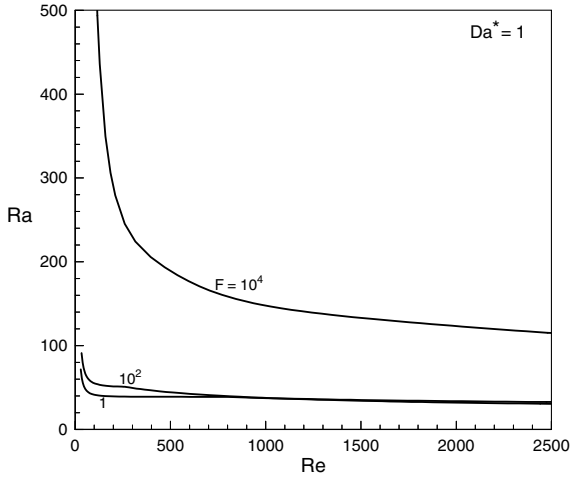

Fig. 2. The instability boundaries on the (Re, Ra)-plane for $Da^* = 1$.

greater than 200. This shows that the Forchheimer number effect on the Ra_c is rather mild for higher modified Darcy number.

The linear instability boundaries for $Da^* = 1$ and $F = 1$, 10^2, and 10^4 on the (Re, α_c) plane, where α_c is the critical streamwise wave number, is plotted in Fig. 3. Those curves demonstrate the variation of α_c with respect to the Re along the neutrally stable curve. It is worth noting that the α_c for $F = 1$ or 10^2 encounters a big upward jump, when the Reynolds number reaches a threshold value. The variation of the α_c value before and after that jump is more than 2 for $F = 1$ and more than 3 for $F = 1$ or 10^2. As discussed later in Table 1, the

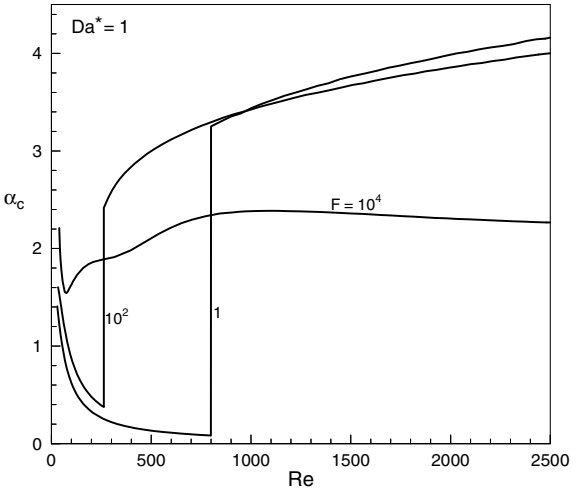

Fig. 3. The variation of wave number, α_c, with Re along the neutral stability curve for $Da^* = 1$.

instability mechanisms are different before and after jump. Before that jump, the instability type is the thermal-buoyant instability. After that jump, the instability type suddenly switches to the thermal-shear instability for $F = 1$ and to mixed instability for $F = 10^2$. Similar characteristic with sudden jump of wave number was found in mixed convection without porous medium in the vertical channel [8,14]. Su and Chung [15] also found such behavior in the linear stability analysis for the vertical heated pipe, where the Chebyshev collocation method was used.

It is also shown in Fig. 3 that the behavior of α_c is different before and after that big jump. Before that jump, the α_c decreases quickly with increasing Reynolds number, while after that jump, the α_c increases with increasing Reynolds number. Each curve has a minimum value, and it is just located at the point where the jump occurs. The Reynolds number, where the α_c has a big jump, is lower when the Forchheimer number is higher, and it occurs at Re about 800 for $F = 1$ and about 263 for $F = 10^2$. After that jump, the α_c's are as high as 2.43 and 3.25 for $F = 1$ and 10^2, respectively, and the α_c's are higher than 4.0 at $Re = 2500$. The behavior of α_c for $F = 10^4$ is different from that of $F = 1$ or 10^2. Its α_c doesn't have a big jump and changes slightly for $Re > 500$, but the curve of α_c also has a minimum value at low Reynolds number. The α_c is greater than 2.0 for $Re > 450$. It is well known that the critical wave number is 1.02 for the isothermal channel flow without porous medium [13]. The above results show that the α_c is greater than 2.0 for most of flow region, which indicates that the wavelength of disturbance in the porous flow is short and it is less half of that for the isothermal channel flow without porous medium.

The wave speed, c_r, along the instability boundary is plotted in Fig. 4, where c_r is the wave speed nondimensionlized by the mean laminar flow velocity. The wave speed curve for $F = 1$ or 10^2 has a downward jump, when the Reynolds number reaches a threshold value, where the α_c also has a big upward jump. After that jump, the c_r increases very slightly with increasing Reynolds number. The wave speed for $F = 10^4$ decreases with increasing Reynolds number, but the rate of decrease is very large for $Re < 300$, while the decrease rate is very small for $Re > 1000$. The wave speeds for all curves are larger than 1, this implies that their wave speeds are larger than the mean fluid velocity.

The instability boundaries on the (Re, Ra) plane for $Da^* = 10^{-2}$ and $F = 1$, 10^2, and 10^4 are plotted in Fig. 5. The results show that all the critical Rayleigh numbers are smaller than 775 for $Re > 200$. This indicates that the fully developed flow could become unstable under a mild heating condition for $Da^* = 10^{-2}$. At the same Re, the Ra_c for $Da^* = 10^{-2}$ is about between 2.0 and 6.0 times of those for $Da^* = 1$. This indicates that the variation of the critical Rayleigh numbers between $Da^* = 1$

Table 1
Energy budget for the neutral stability curve (TS: thermal-shear instability, M: mixed instability, TB: thermal-buoyant instability)

Re	Ra_c	α_c	Da^*	F	E_s	E_b	E_{Da}	E_F	E_d	Type
100	41.4	0.62	1	1	0.066	0.934	−0.065	−0.006	−0.929	TB
798	38.85	0.084	1	1	0.037	0.963	−0.061	−0.006	−0.932	TB
802	38.83	3.25	1	1	0.824	0.176	−0.025	−0.002	−0.973	TS
1500	35.1	3.76	1	1	0.899	0.101	−0.020	−0.002	−0.978	TS
2500	32.7	4.16	1	1	0.936	0.064	−0.017	−0.001	−0.982	TS
100	55.1	0.87	1	10^2	0.180	0.820	−0.045	−0.299	−0.656	TB
261	50.9	0.376	1	10^2	0.172	0.828	−0.042	−0.311	−0.647	TB
265	50.8	2.43	1	10^2	0.548	0.452	−0.031	−0.184	−0.785	M
800	39.7	3.29	1	10^2	0.819	0.181	−0.023	−0.150	−0.828	TS
1500	34.2	3.67	1	10^2	0.897	0.103	−0.019	−0.137	−0.844	TS
2500	30.5	4.00	1	10^2	0.935	0.067	−0.016	−0.126	−0.858	TS
200	288.6	1.85	1	10^4	0.066	0.934	−0.009	−0.839	−0.152	TB
800	158.4	2.34	1	10^4	0.303	0.697	−0.007	−0.801	−0.192	M
1500	133	2.36	1	10^4	0.521	0.479	−0.007	−0.785	−0.208	M
2500	115	2.27	1	10^4	0.667	0.333	−0.006	−0.781	−0.213	M
3750	98.1	2.22	1	10^4	0.754	0.246	−0.006	−0.777	−0.217	TS
5000	85.2	2.21	1	10^4	0.804	0.196	−0.006	−0.773	−0.221	TS
200	324.3	1.64	10^{-2}	1	0.135	0.865	−0.835	−0.000	−0.165	TB
800	124.8	2.32	10^{-2}	1	0.453	0.547	−0.765	−0.000	−0.235	M
1500	96.9	2.35	10^{-2}	1	0.672	0.328	−0.750	−0.000	−0.250	M
2500	75.6	2.36	10^{-2}	1	0.792	0.208	−0.741	−0.000	−0.259	TS
3750	58.9	2.41	10^{-2}	1	0.858	0.142	−0.731	−0.000	−0.269	TS
5000	48.3	2.48	10^{-2}	1	0.893	0.107	−0.722	−0.000	−0.278	TS
200	774.9	1.58	10^{-2}	10^4	0.040	0.960	−0.594	−0.277	−0.277	TB
800	239.7	2.00	10^{-2}	10^4	0.230	0.770	−0.507	−0.344	−0.344	TB
1500	182.8	2.20	10^{-2}	10^4	0.434	0.566	−0.481	−0.346	−0.346	M
2500	157.7	2.14	10^{-2}	10^4	0.605	0.395	−0.466	−0.353	−0.353	M
3750	136.3	2.06	10^{-2}	10^4	0.708	0.292	−0.457	−0.361	−0.361	TS
5000	118.8	2.04	10^{-2}	10^4	0.766	0.234	−0.449	−0.365	−0.365	TS
300	3780800	8.12	10^{-4}	1	−0.022	1.022	−0.820	−0.000	−0.180	TB
800	947400	5.27	10^{-4}	1	−0.063	1.063	−0.870	−0.000	−0.130	TB
1500	442650	3.94	10^{-4}	1	−0.080	1.080	−0.894	−0.000	−0.106	TB
2500	249550	3.05	10^{-4}	1	−0.088	1.088	−0.913	−0.000	−0.087	TB
3750	160400	2.41	10^{-4}	1	−0.088	1.088	−0.931	−0.000	−0.069	TB
5000	116400	2.01	10^{-4}	1	−0.078	1.078	−0.944	−0.000	−0.056	TB

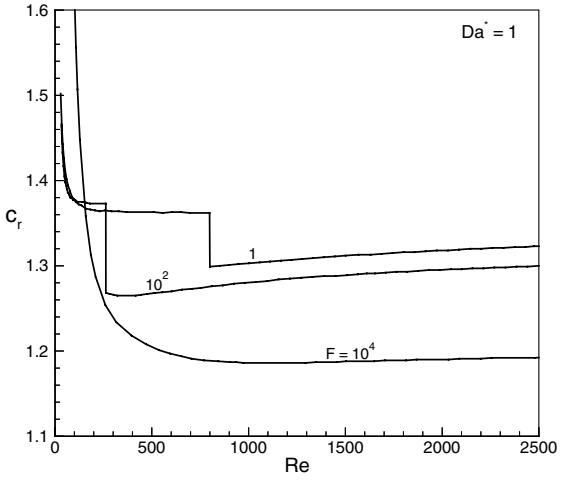

Fig. 4. The variation of wave speed, c_r, with Re along the neutral stability curve for $Da^* = 1$.

and 10^{-2} is within one order of magnitude. The Ra_c in Fig. 5 decreases with increasing Reynolds number, and the rate of decrease is smaller for higher Re. The curves for $F = 1$ and 10^2 are almost overlapping each other. The critical Rayleigh number for $F = 10^4$ is only about 1.8 times larger than that of $F = 1$ or 10^2. This indicates that the Forchheimer number effect on the Ra_c is small for $Da^* = 10^{-2}$.

The linear instability boundaries for $Da^* = 10^{-2}$ on the (Re, α_c) plane is plotted in Fig. 6 for $F = 1$, 10^2, and 10^4. Each curve doesn't have any sudden jump, while the α_c has a big jump for $Da^* = 1$ and $F = 1$ or 10^2, as shown before in Fig. 3. But each curve in Fig. 6 also has a minimum value at low Reynolds number, it occurs at Re about 120 for $F = 1$ and 10^2, and about 150 for $F = 10^4$. Before that minimum value, the α_c decreases quickly with the increase of Re. After that point, the α_c initially increases quickly with the increase of Re and

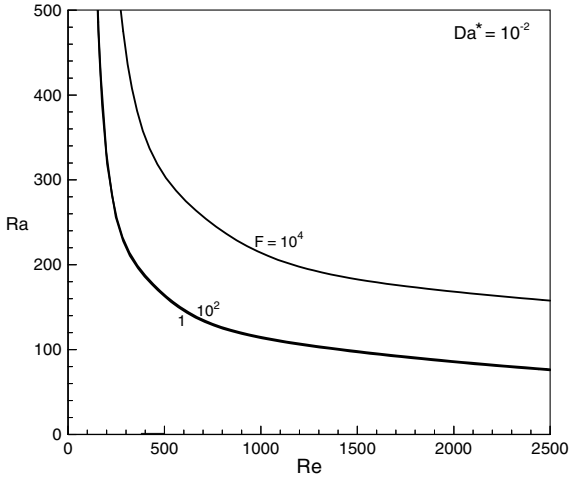

Fig. 5. The instability boundaries on the (Re, Ra)-plane for $Da^* = 10^{-2}$.

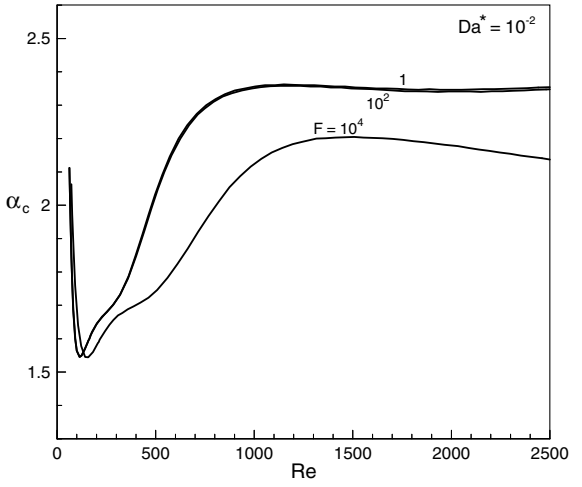

Fig. 6. The variation of wave number, α_c, with Re along the neutral stability curve for $Da^* = 10^{-2}$.

then generally levels off. The α_c changes little and its value falls between 2 and 2.4, when the Reynolds number is greater than about 1000. This indicates that for most of flow region the wavelength of disturbances for $Da^* = 10^{-2}$ is less half of the wavelength of the isothermal channel flow without porous medium (with α_c of 1.02). The variation of wave speed, c_r, with the Reynolds number is plotted in Fig. 7. The c_r of each curve decreases very quickly with increasing Re at low Re region. The wave speed changes very small for $Re > 1000$ and its value is about 1.2.

The critical Rayleigh number is substantially increased for $Da^* = 10^{-4}$ and three curves for $F = 1$, 10^2, and 10^4 are almost overlapping each other, as shown in Fig. 8. This indicates that the effect from Forchheimer number is negligible for $F \leqslant 10^4$. At $Re = 2500$, the Ra_c for $Da^* = 10^{-4}$ is as high as about 249,500, while the Ra_c for $Da^* = 10^{-2}$ is 157.7 for $F = 10^4$. This shows that Ra_c of $Da^* = 10^{-4}$ is about 1580 times larger than that of $Da^* = 10^{-2}$. At $Re = 300$, the Ra_c for $Da^* = 10^{-4}$ is as high as about 3.781×10^6, which is 8400 times larger than that of $Da^* = 10^{-2}$. In other word, the Ra_c for $Da^* = 10^{-4}$ is three to four orders larger than that of $Da^* = 10^{-2}$ at the same Re. It is reminded that the variation of Ra_c between $Da^* = 1$ and 10^{-2} is less than one order magnitude at the same Re. As shown later in Table 1,

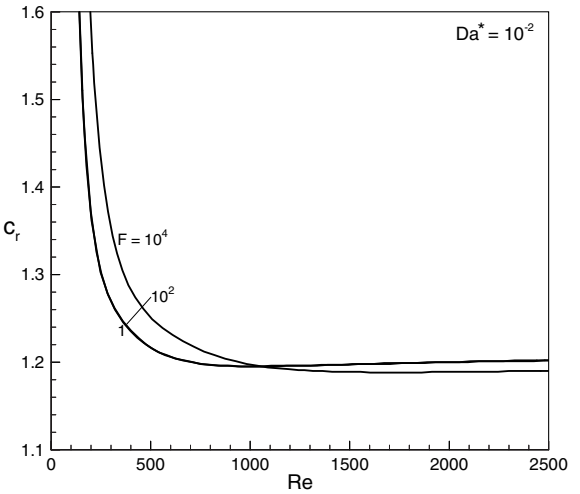

Fig. 7. The variation of wave speed, c_r, with Re along the neutral stability curve for $Da^* = 10^{-2}$.

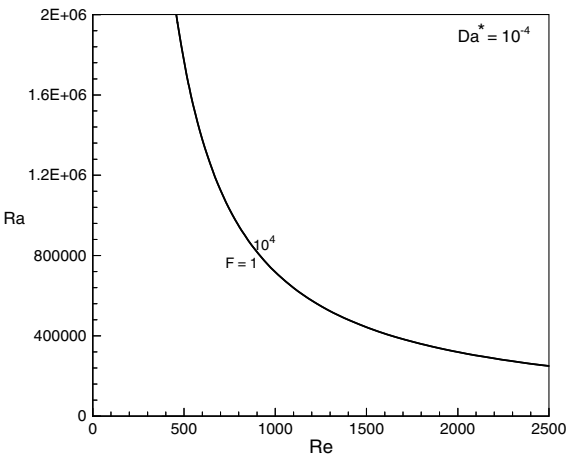

Fig. 8. The instability boundaries on the (Re, Ra)-plane for $Da^* = 10^{-4}$.

the thermal-buoyant instability is the only type for the flow instability regardless of the value of Re for $Da^* = 10^{-4}$, while there are generally three instability types for different Reynolds numbers for $Da^* = 1$ and 10^{-2}. This indicates that the modified Darcy number has an important effect on the flow instability.

The variation of the critical wave number, α_c, with the Reynolds number along the neutrally stable curve is shown in Fig. 9 for $Da^* = 10^{-4}$. Its behavior is also substantially different from that of $Da^* = 1$ or 10^{-2}. The α_c for $Da^* = 10^{-4}$ decreases monotonously with increasing Reynolds number, while all the wave number curves for $Da^* = 1$ or 10^{-2} have a minimum value, as shown before in Figs. 3 and 6. It is also seen in Fig. 9 that the α_c at low Re is high and it is as high as 8.12 at $Re = 300$. Its wavelength of disturbance in is only 0.13 of that for the isothermal channel flow without porous medium. This shows that the wavelength of disturbance for $Da^* = 10^{-4}$ is rather short at low Reynolds number. This indicates that its instability is caused by a local disruption of the velocity field, which is induced by the temperature fluctuation. Fig. 9 also shows that all the α_c's are greater than 2.0. The variation of the wave speed, c_r, with the Reynolds number for $Da^* = 10^{-4}$ is shown in Fig. 10. The wave speed decreases monotonically with increasing Reynolds number. It is seen that the c_r's are as high as 12.6 and 4.19 for $Re = 300$ and 2500, respectively, while they are only about 1.27 and 1.2 for $Re = 300$ and 2500, respectively, for $Da^* = 10^{-2}$. This indicates that the wave speed for $Da^* = 10^{-4}$ is significantly higher than that of $Da^* = 1$ or 10^{-2}.

The analysis of kinetic energy transfer budget for the neutral stability curve, as shown in Eq. (15), could provide some insights on the transport mechanisms during flow instability. As summary of the energy budget is given in Table 1. For $Da^* = 1$ and $F = 1$ or 10^2, it is reminded that the α_c encounters a big jump, when the Reynolds number reaches a threshold value (about 800 for $F = 1$ and about 263 for $F = 10^2$), as shown in Fig. 3. It is seen in Table 1 that the instability type before that big jump is the thermal-buoyant instability, where the kinetic energy mainly comes from the shear production, E_s. After that jump, the instability type suddenly switches from the thermal-buoyant instability to the thermal-shear instability for $F = 1$ or to mixed instability for $F = 10^2$. It is noted that for the thermal-shear instability, the kinetic energy mainly comes from the shear production, E_s. For the mixed instability, the energy generations from shear and buoyant forces are in the same order. In this paper, the mixed instability is loosely defined as that either the E_s or E_b shears 30–70% of the total kinetic energy production. At high Reynolds number, the instability type is the thermal-shear instability. For $F = 10^4$ ($Da^* = 1$), the instability mechanism is different from that for $F = 1$ or 10^2. The instability types are the thermal-buoyant, mixed, and thermal-shear instabilities for low, intermediate, and high Reynolds numbers, respectively. For $F = 1$ or 10^2, the kinetic energy is mainly dissipated through the viscosity term, E_d, while it is mainly dissipated through Forchheimer term (due to the form drag of solid matrix), E_F, for $F = 10^4$.

The instability mechanisms for $Da^* = 10^{-2}$ and $F = 1 - 10^4$ are similar. The instability type is the thermal-buoyant instability at low Reynolds number. It is seen that the kinetic energy generated from the shear production, E_s, gradually increases with increasing Reynolds number. At the same Re, the shear production is also higher when the Forchheimer number is smaller. Therefore the instability type gradually switches to the mixed instability for intermediate Re, and finally

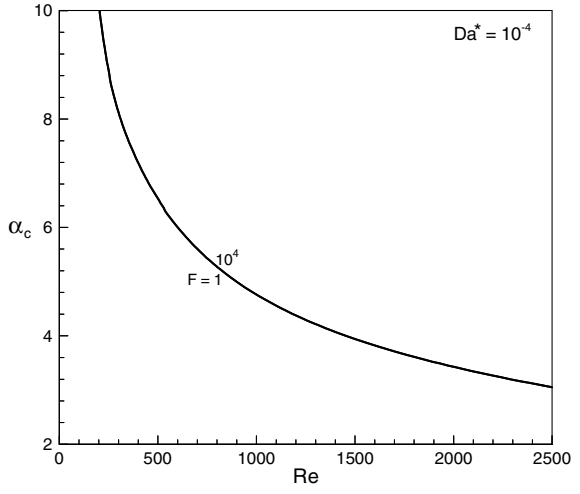

Fig. 9. The variation of wave number, α_c, with Re along the neutral stability curve for $Da^* = 10^{-4}$.

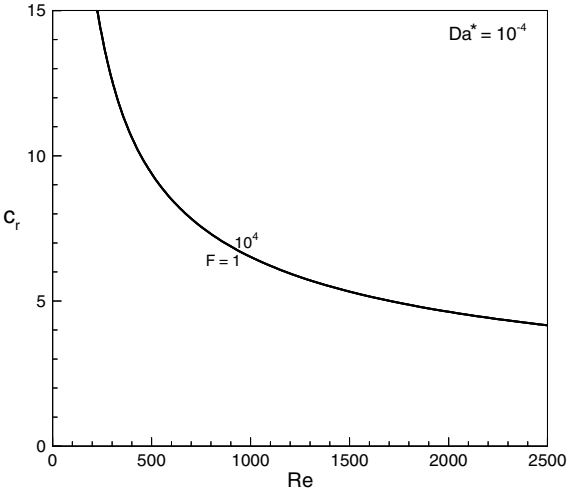

Fig. 10. The variation of wave speed, c_r, with Re along the neutral stability curve for $Da^* = 10^{-4}$.

becomes to the thermal-shear instability at high Re. The transition from one instability type to another type is also gradually. This indicates that there are generally three types of instability mechanisms for higher modified Darcy number. For $F = 1$ or 10^2, the kinetic energy is now mainly dissipated through the modified Darcy term (due to the surface drag of solid matrix), E_{Da}, while few of kinetic energy is dissipated through the viscosity term, E_d. It is seen that E_F (due to Forchheimer term) is almost zero regardless of the Reynolds number. For $F = 10^4$, the kinetic energy is generally dissipated through all the three terms of E_{Da}, E_F, and E_d, even though E_{Da} is larger than E_F or E_d.

The instability mechanism for $Da^* = 10^{-4}$ is very different from those of $Da^* = 1$ or 10^{-2}. The thermal-buoyant instability is the only type for the flow instability regardless of the value of Reynolds number, while there are generally three instability types for $Da^* = 1$ or 10^{-2}. It is reminded that the critical Rayleigh number for $Da^* = 10^{-4}$ is significantly larger than that for $Da^* = 1$ or 10^{-2}. This result can be realized from what happens when the modified Darcy number tends to zero. In this limit the flow would be slug flow for pure forced convection, no matter what the value of F, and such flow is always stable. This asymptotic limit would be nearly attained for $Da^* = 10^{-4}$. This explains why only the thermal-buoyant type of instability is possible for $Da^* = 10^{-4}$ in the mixed convection, where the kinetic energy generated from the buoyancy force is the only driving mechanism for the flow instability. Also, it is worth pointing out that when modified Darcy number is very small, the base velocity and temperature profiles are mainly a function of Rayleigh–Darcy number ($Ra \times Da^*$), which can be deduced from Eqs. 5 and 6 in Ref. [4]. Thus it is the Rayleigh–Darcy number rather than Ra that is pertinent for very small Da^*. It is also showed in Table 1 that more than 82% of the kinetic energy for $Da^* = 10^{-4}$ is dissipated through the modified Darcy term of E_{Da}, and the E_{Da} is larger for higher Re. The energy dissipation through E_F is almost zero regardless of the Reynolds number.

6. Conclusions

The linear stability analysis of mixed convection in a heated vertical channel filled with a fluid-saturated porous medium with imposing uniform heat flux at the plates was investigated by using Darcy–Brinkman–Forchheimer model. The results showed that the modified Darcy number, Da^*, has an important effect on the flow stability characteristics. The lower of the modified Darcy number, the higher of the critical Rayleigh number, Ra_c. For higher value of Da^*, the variation of Ra_c between $Da^* = 1$ and 10^{-2} is mild (within one order of magnitude) at the same Reynolds number, and all the Ra_c's are less than 775 for $Re > 200$. This indicates that the fully developed flow for higher modified Darcy number could become unstable under a mild heating condition. For lower value of $Da^* = 10^{-4}$, the Ra_c is significantly increased, and its Ra_c is three to four orders larger than that of $Da^* = 10^{-2}$ at the same Re. The effect of Forchheimer number, F, on the Ra_c is mild. It is also found that the disturbance with zero spanwise wave number is always the least stable mode, that is, the least stable disturbances are two-dimensional.

The disturbance kinetic energy budget analysis showed that the driving mechanisms are substantially different between the higher and lower modified Darcy number. For higher value of $Da^* = 1$ or 10^{-2}, there are generally three instability types, the thermal-buoyant, mixed, and thermal-shear instabilities for low, intermediate, and high Reynolds numbers, respectively. While for lower value of $Da^* = 10^{-4}$, the thermal-buoyant instability is the only type for the flow instability regardless of the value of Reynolds number, which indicates that the kinetic energy generated from buoyancy force is responsible for the flow instability.

The critical wave number, α_c, is generally greater than 2.0 for most of flow region. This indicates that the wavelength of disturbance for mixed convection in the porous flow is short and it is generally less half of that for the isothermal channel flow without porous medium (with α_c of 1.02). The result from the variation of α_c with Re showed that the α_c for $Da^* = 1$ and $F = 1$ or 10^2 encounters a big upward jump, when the Reynolds number reaches a threshold value. The α_c and instability type show a different behaviors before and after that jump. Before that jump, the α_c decreases quickly with increasing Re, and it is the thermal-buoyant instability. After that jump, the α_c increases slowly with increasing Re, and the instability type suddenly switches to the thermal-shear instability for $F = 1$ and to mixed instability for $F = 10^2$.

The instability characteristics for $Da^* = 1$ and $F = 10^4$, and $Da^* = 10^{-2}$ and $F = 1$–10^4 are generally similar. But their wave number curves do not have sudden jump. The transition from one instability type to another type is also gradually. The result also indicated that all the curves of α_c's have a minimum value for the higher modified Darcy number of $Da^* = 1$ or 10^{-2}. While the critical wave number for $Da^* = 10^{-4}$ shows different behavior, its α_c is very large at low Re and it decreases monotonously with increasing Reynolds number.

Acknowledgements

This research work was partially supported by National Science Council, Taiwan, ROC, under grant NSC

88-2621-B-161-001. The computing resource was provided by National Center for High-Performance Computing, Taiwan, ROC. The author is thankful to one reviewer's comment about the instability mechanism when the Darcy number tends to zero. This comment has been added in the discussions of the kinetic energy budget analysis.

References

[1] K. Vafai, S.J. Kim, Forced convection in a channel with a porous medium: an exact solution, ASME J. Heat Transfer 111 (1989) 1103–1106.
[2] D.A. Nield, S.L.M. Junqueira, J.L. Large, Forced convection in a fluid-saturated porous-medium channel with isothermal or isoflux boundaries, J. Fluid Mech. 322 (1996) 201–214.
[3] A. Hadim, G. Chen, Non-Darcy mixed convection in a vertical porous channel, J. Thermophys. Heat Transfer 8 (1994) 805–808.
[4] Y.C. Chen, J.N. Chung, C.S. Wu, Y.F. Lue, Non-Darcy mixed convection in a vertical channel filled with a porous medium, Int. J. Heat Mass Transfer 43 (2000) 2421–2429.
[5] D.A. Nield, A. Bejan, Convection in Porous Media, second ed., Springer-Verlag, New York, 1999.
[6] H.H. Bau, K.E. Torrance, Onset of convection in a permeable medium between vertical coaxial cylinders, Phys. Fluids 24 (1981) 382–385.
[7] N. Kladias, V. Prasad, Flow transitions in buoyancy-induced non-Darcy convection in a porous medium heated from below, J. Heat Transfer 112 (1990) 675–684.
[8] Y.C. Chen, J.N. Chung, The linear stability of mixed convection in a vertical channel flows, J. Fluid Mech. 325 (1996) 29–51.
[9] Y.C. Chen, J.N. Chung, A direct numerical simulation of K- and H-type flow transition in a heated vertical channel, Phys. Fluids 14 (2002) 3327–3346.
[10] R.C. Givler, S.A. Altobelli, A determination of the effective viscosity for the Brinkman–Forchheimer flow model, J. Fluid Mech. 258 (1994) 355–370.
[11] T.S. Lundgren, Slow flow through stationary random beds and suspensions of spheres, J. Fluid Mech. 51 (1972) 273–299.
[12] S.A. Orszag, Accurate solution of the Orr–Sommerfeld stability equation, J. Fluid Mech. 50 (1971) 689–703.
[13] J.E. Hart, Stability of the flow in a differentially heated inclined box, J. Fluid Mech. 47 (1971) 547–576.
[14] Y.C. Chen, J.N. Chung, Stability of mixed convection in a differentially heated vertical channel, ASME J. Heat Transfer 120 (1998) 127–132.
[15] Y.C. Su, J.N. Chung, Linear stability analysis of mixed convection flow in a vertical pipe, J. Fluid Mech. 422 (2000) 141–166.